Person Re-Identification using Deep Foreground Appearance Modelling

Gregory Watson & Abhir Bhalerao

Abstract

Person Re-Identification is the process of matching individuals from images taken of them at different times, and often with different cameras. To perform matching, most methods extract features from the entire image, however, this gives no consideration to the spatial context of the information present in the image. In this paper, we propose using a convolutional neural network approach based on ResNet-50 to predict the foreground of an image: the parts with the head, torso and limbs of a person. With this information, we use the LOMO and Salient Colour Name feature descriptors to extract features primarily from the foreground areas. In addition, we use a distance metric learning technique (XQDA), to calculate optimally weighted distances between the relevant features. We evaluate on the VIPeR, QMUL GRID and CUHK03 data sets, and compare our results against a linear foreground estimation method, and show competitive or better overall matching performance.

*Gregory Watson, g.a.watson@warwick.ac.uk

1 Introduction

Person Re-Identification (Re-ID) is the process of identifying an individual from a gallery of images which also contains at least one image of that person. It has several important applications, including but not limited to,

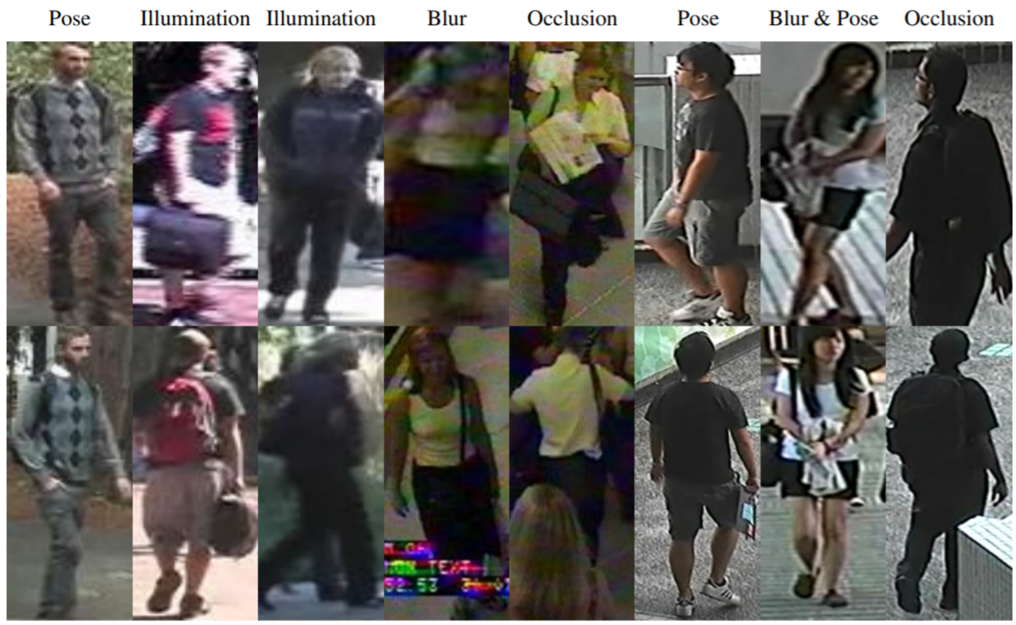

Figure 1: Examples of various images from the VIPeR [1], QMUL GRID [2, 3, 4] and CUHK03 [5] data sets. Each column represents a single identity.

surveillance, biometrics and security. However, variations in illumination, background, pose and resolution present significant challenges to Person Re-Identification techniques (see illustrated examples in Fig 1).

Specifically, pose variation can lead to two images of the same individual looking significantly different depending on the pose of their body, but also of the direction from which the image is taken, e.g. from the front or behind, from above or from one side. A network of CCTV cameras positioned at different locations in a pedestrian area will inevitably exhibit large differences in a person's pose between the images. Matching images of people with different poses is problematic as corresponding features regions do not represent the same things. To overcome this, several techniques have been proposed; for example, Yang, Yang et. al [6] split the image into a series of stripes which allows for feature extraction and matching to be carried out on an area-by-area basis, and has been shown to improve matching results. Liu, Chunxiao and Gong [7] also divide images into stripes but then go on to weight different feature types according to a stripe's content. They measure textural and non-textural (colour) content and so, for example, a person's patterned clothing will have higher texture weighting than that which is plain coloured.

Other approaches use a model to identify which areas constitute the foreground, such as the body as a whole, or labelling regions at the level of limbs. Symmetry-Driven Accumulation of Local Features (SDALF) [8] divides a person image into three parts - the head, torso and legs, and following this, a vertical axis of symmetry is estimated as the axis which best separates appearances on either side of it. STEL Component Analysis [9] attempts to capture the structure of each image by splitting it into parts (so called stels) which have a similar distributions of features. However, if multiple different parts of the image have a similar feature distribution, and these lie both in the foreground and background, then the separation may work poorly.

Recently [10], we proposed an appearance based method for estimating the pose of a person using a linear regression of image HOG features to coordinates and widths of a skeleton model. A Partial Least-Squares (PLS) regression model was calculated using supervised data and we were able to show a significant increase in matching results when compared with other foreground modelling methods.

Convolutional Neural Networks (CNNs) have also been used for foreground modelling in person Re-ID. Cheng, Gong et al. [11] propose using a multi-channel CNN to learn both global image features and local body-part features defined by four stripes in each image, and so it does not give consideration to which areas are foreground and which are background. Zhao, Tian et al. [12] propose a network which locates fourteen points on a person image locating the joints of a person's skeleton. These points can then be used to define the bounding boxes of limbs. GLAD [13] takes advantage of the DeeperCut [14] pose estimation method, which uses a 152-layer network to predict a series of skeleton key-points. It then uses a subset of these key-points to divide a person image into three areas - head, upper-body and lower-body. Liu, Lyu et al. [15] also train a CNN using both original images and semantic segmentation probability maps obtained via the DeepLab [16] model. With both of these inputs, the authors demonstrate a high performance when compared to only using the original images, and are able to predict skeletons with high accuracy. However, the method does not distinguish between different limbs, making matching between them impossible.

Once a foreground area has been estimated, the next stage is Feature Extraction. Liao, Hu et al. [17] proposed Local Maximal Occurrence (LOMO), which splits each image into 10×10 pixel patches with a 5 pixel overlap in each dimension. A HSV Joint Histogram and an SILTP texture histogram [18] are extracted from each patch. For each row of patches, the highest value in each histogram bin is taken as the value for that bin in the final descriptor. Yang et al. [6] proposed Salient Colour Names, where sixteen colour names are defined in the RGB colour space, and each pixel value is quantised based on its distance to these sixteen points. This allows a descriptor to be built where each pixel can be defined as an amount of each of the sixteen colours. However, the authors argue that features extracted from the background areas can be important to provide context, and therefore extract features from both whilst providing priority to the foreground features. Our proposed algorithm too uses the LOMO and Salient Colour Names features, but weighting foreground features higher, and using a body part based partitioning of the foreground.

The main contribution of this paper is a foreground modelling method which uses a Deep CNN to learn a regression between the input images and ground-truth, hand-labelled skeletons. As well as regressing to the skeleton joint locations, the model is also trained to learn the widths of the limbs. After predicting the skeleton of an unseen person image, we extract features primarily from the foreground area, minimising the problem of background information being used to build the feature descriptors. We evaluate our methods on the VIPeR [1], QMUL GRID [2, 3, 4] and CUHK03 [5] data sets and compare the accuracy of the skeleton fitting with linear appearance based methods [10]. We incorporate both methods into a matching framework with LOMO, Salient Colour Names and distance metric learning to demonstrate improved Rank-1 matching rates. We draw some initial conclusions and suggest how a deep skeleton fitter may be used in a fully deep neural network matching framework.

2 Method

In this section, we detail our Deep CNN method, which is trained to predict the location of a person's skeleton from Re-ID images. The output is used to estimate foreground regions of an image and locations of the head, torso and limbs. We used these areas to locally extract features for matching.

2.1 Deep Appearance Modelling

For a given training set of identities, we pass all images and corresponding ground-truth, hand-labelled skeletons to our network. Given the small number of identities and images per identity in most Re-ID data sets versus the large number required for training a CNN model, we apply data augmentation to increase the size of the training set. For all images in the training set, we create additional images and corresponding skeletons by applying various small rotations, translations and horizontal flips (reflection in the y-axis).

Each skeleton is defined by a set of labeled points, which represent the position of the head, torso and limbs (arms and legs), 15 (x, y) key-points in total; the arms and legs consist of three sections each with a width variable; and the torso is also given a width. Widths are defined by 14 key-points at positions perpendicular to a limb section axis, at the end of the section (see

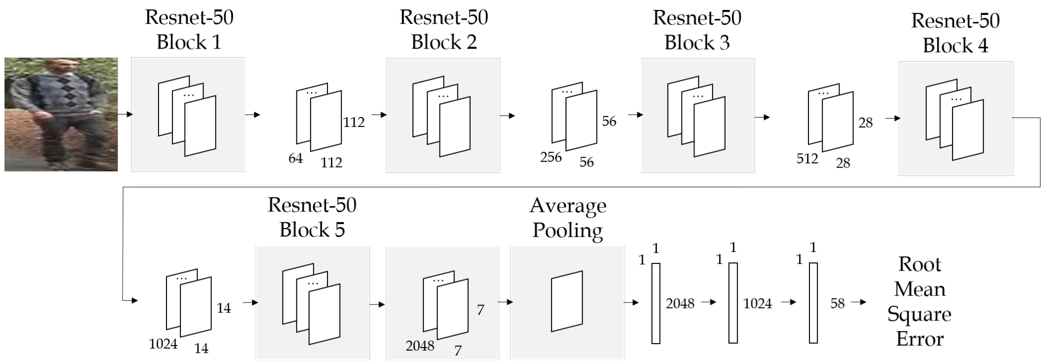

Figure 2: The network architecture for our proposed deep foreground modelling method. Images are re-scaled to 224×224 pixels and passed through the convolutional layers of the ResNet-50 network [19]. We take the POOL5 Average Pooling layer as output of the ResNet-50 model, flatten the output, and finally concatenate with two Fully Connected layers. The output layer contains 58 units representing the (x, y) coordinates of skeleton key-points (joints and width markers). We use the RMSProp [20] optimizer and a Mean Squared Error Loss.

Fig 3).

The CNN takes a Re-ID image as input and outputs the key-point locations as output. To take advantage of transfer learning, we use pre-trained weights from the ResNet-50 architecture [19] and therefore all input images are resized to have resolutions 224×224 pixels. The fully connected layers of this network are modified and we replace them with fully-connected layers of size 1024 and then the output layer with size 58, see Fig 2.

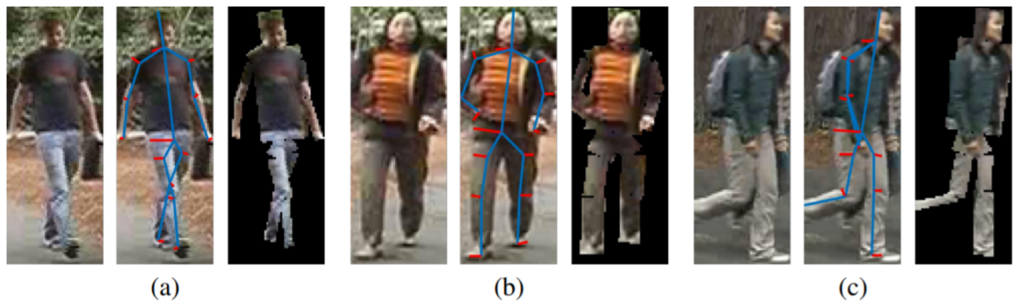

Figure 3: Three examples of a triplet of original images, a skeleton and an image mask that can be produced from the skeleton. Any part of the image within the image mask is considered foreground.

2.2 Foreground feature extraction and feature weighting

Given a predicted skeleton, an image mask/silhouette of a person is generated by taking rectangular regions for the torso and limb sections (given the joint key-point locations and the width markers). Examples of skeletons and their corresponding image masks can be seen in Fig 3. The predicted foreground area is then used to localise the calculation of two types of image features: LOMO [17] features and Salient Colour Names [6] features.

2.2.1 LOMO and Weighted LOMO

LOMO [17] features consist of joint HSV histograms and SILTP [18] histograms over three scales, and are extracted from 10×10 pixel patches with a 5 pixel overlap in each dimension. For each row of patches, the maximum value in each histogram bin is taken as the final descriptor. As in our previous work [10], we modify LOMO so that features are primarily extracted from the foreground areas. Each patch is weighted by the percentage of predicted foreground pixels within the patch:

$$\mathbf{f}_w(B) = \frac{|F \cap B|}{|B|}\mathbf{f}(B), \tag{1}$$

where B is all pixels within the patch, and F is all pixels labelled foreground. Therefore, for each row, the maximum value for each histogram bin is more likely to be taken from the foreground area. We concatenate these features and the original LOMO features to create Weighted LOMO.

2.2.2 Salient Colour Names

Salient Colour Names [6] features defines sixteen coordinates in the RGB colour space which each represent a colour, such as fuchsia, blue, aqua and lime etc. The process is a form of vector quantisation, creating a mapping from pixel values in the RGB colour space to a colour name distribution amongst a set of fixed colours. We extract a sixteen-bin Salient Colour Names histogram from each limb of our predicted person skeleton, apply a log transform, and normalise it to unit length. We then concatenate these features to form our final feature descriptor. By localising to limbs, the colour features are made approximately person-pose invariant: different parts of the colour feature vector representing a person's clothing, distinguishing tops from trousers, shorts and skirts.

2.3 Distance Metric Learning

Distance Metric Learning (DML) is a way to find a subspace mapping of features in which distances between matching identities is minimised. KISSME [21] was the first major DML used for Person Re-Identification, and it calculates the distance between two feature vectors as:

$$\tau_M^2(\mathbf{f_i}, \mathbf{f_j}) = (\mathbf{f}_i - \mathbf{f}_j)^T (\Sigma_I^{-1} - \Sigma_E^{-1})(\mathbf{f}_i - \mathbf{f}_j). \tag{2}$$

where the intra-personal, Σ_I, and extra-personal, Σ_E, scatter matrices are sample estimates from training data. Several methods have since expanded on KISSME, such as Cross-view Quadratic Discriminant Analysis (XQDA) [17]. Whereas KISSME applies PCA to the input vectors prior in estimating Σ_I and Σ_E, giving no regard to the relationship between DML and dimensionality reduction stages, XQDA performs DML and dimensionality reduction stages together. If D is the original dimensionality of the data, and R the reduced dimensionality, XQDA learns a subspace $W = (\mathbf{w}_1, \mathbf{w}_2, ..., \mathbf{w}_R) \in \mathbb{R}^R$, whilst simultaneously learning a distance function:

$$d_w(\mathbf{f}_i, \mathbf{f}_j) = (\mathbf{f}_i - \mathbf{f}_j)^T W(\Sigma_I'^{-1} - \Sigma_E'^{-1}) W^T (\mathbf{f}_i - \mathbf{f}_j) \tag{3}$$

where $\Sigma_I' = W^T \Sigma_I W$ and $\Sigma_E' = W^T \Sigma_E W$. Using the the Generalised Rayleigh Quotient

$$J(\mathbf{w}) = \frac{\mathbf{w}^T \Sigma_E \mathbf{w}}{\mathbf{w}^T \Sigma_I \mathbf{w}} \tag{4}$$

as the objective function, it can be shown that the solution vectors $\mathbf{w}$ are found by a generalised eigenvalue decomposition by maximising:

$$\max_{\mathbf{w}} \mathbf{w}^T \Sigma_E \mathbf{w}, \ s.t. \ \mathbf{w}^T \Sigma_I \mathbf{w} = 1. \tag{5}$$

Here, for training the XQDA Distance Metric, we use the features extracted from the sets of training images, using the ground-truth skeletons.

3 Results and Discussion

We investigate the performance of our methods on three of the main Re-ID data sets:

- VIPeR [1] consists of 632 image pairs, captured using two different cameras. Images have a resolution of 128×48 pixels, and exhibit large variation in pose and illumination.

- QMUL GRID [2, 3, 4] consists of 250 image pairs taken using eight different cameras in an underground rail system. In addition, there are 775 additional images which do not share an identity with an individual from the 250 image pairs. Images from the QMUL GRID data set have various different aspect ratio and resolutions, and suffer from large variation in pose and illumination. Additionally, occlusion and image capture noise are common in this data set.

- CUHK03 [5] is a larger data set, consisting of 1467 people with up to ten images per person, taken from a series of camera pairs at various image resolutions. As the images were taken over a period of several months, large variation in illumination is seen. This data set also suffers from significant pose variation and occlusion.

For all three data sets, we initially train the fully-connected layers of our ResNet-50 based CNN using pre-trained weights, and follow by training all layers from ResNet-50's third stage onwards. We use the RMSProp [20] optimizer with a learning rate of 0.001.

We split VIPeR in to 316 training/validation identities and 316 testing identities. We randomly assign 80% of the training/validation identities as training identities, and the remaining for validation. As deep approaches require more data than traditional ones, so we expand the size of the training and validation sets by taking all images from the QMUL GRID data set. For QMUL GRID, we split the identities into two sets - those which form an image pair and those which do not form a pair. We then take 80% of each set for training and 20% for validation. Separating the identities in this way allows us to have a consistent number of training and validation images between folds. We train for fifteen epochs with a batch size of 32. After skeleton prediction, we resize all images to the standard resolution of 128×48 pixels, rescaling all skeletons to the new size. Examples of the skeleton fitting on the VIPeR data set can be seen in Fig 4. Following the skeleton fitting and feature extraction, due to the XQDA distance metric learning stage requiring no validation set, we combine the training and validation sets to learn the

Distance Metric. We run our experiments ten times, averaging to produce the final results.

From Table 1, we can see that our Deep Neural-Network Appearance Modelling (DNAM) method performs better than other methods at Rank-10 and Rank-20, but does not perform as well our Partial Least Squares (PLSAM) method at Rank-1 and Rank-5. When compared to using only the original LOMO features, we can see an increase of 5.0% in the Rank-1 rate, but a decrease of 1.0% when compared to the PLS skeleton fitting. We believe that this is because the skeleton fitting between both PLS and Deep CNN methods are similar, with the Deep Network method having a lower average Root Mean Squared Error. The CMC curve can be seen in Fig 6.

For QMUL GRID, we split the data set into 125 training/validation identities and 125 testing identities, with all images of identities which do not belong to an image pair being added to the testing gallery set. We supplement the training/validation set with the entirety of the VIPeR data set, and again assign 80% of the identities from the combined data set as training identities, with the remaining being validation identities. Also, similar to the experimentation on the VIPeR data set, we combine the training and validation sets when undertaking the DML step. We train for ten epochs with

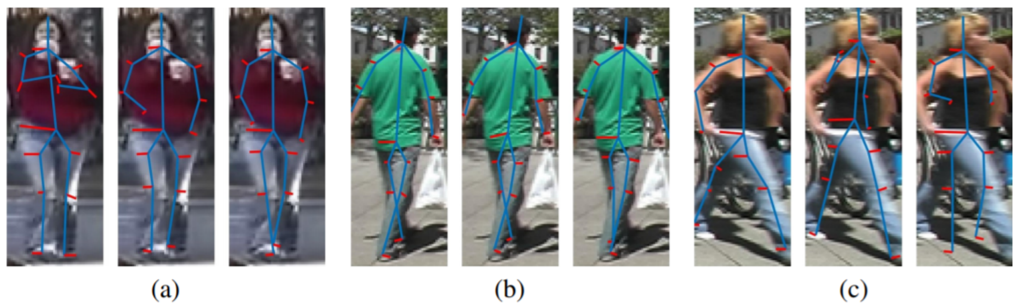

Figure 4: Examples of ground-truth, deep predicted skeletons and PLS predicted skeletons on the VIPeR [1] data set: (a) An example image with a RMSE of 6.5 pixels when using the deep method, and 7.6 pixels when using the PLS method; (b) The image with the minimum RMSE when using the deep method of 1.5 pixels, with the same image having an RMSE of 2.9 pixels when using the PLS method; (c) The image with the maximum RMSE when using the deep method of 17.9 pixels, with the same image having an RMSE of 12.3 pixels when using the PLS method. The average RMSE when using the deep method was 4.5 pixels, with the average when using the PLS method being 5.2 pixels.

a batch size of 16. After skeleton prediction, we again resize all images to the standard resolution of 128×48 pixels, rescaling all skeletons accordingly. Examples of the skeleton fitting on the QMUL GRID data set can be seen in Fig 5. We again run our experiments ten times, averaging to produce the final results.

From Table 1, we can see that the best results are obtained from the Deep CNN based skeleton fitter. When compared to using only the original LOMO features, we achieve a 11.1% increase in the Rank-1 rate, and an increase of 1.7% when compared to the highest result from the PLS method. We can

	VIPeR				QMUL GRID			
	r=1	r=5	r=10	r=20	r=1	r=5	r=10	r=20
DNAM(v2)	45.3	74.8	**86.4**	**94.2**	**28.4**	**49.2**	**60.0**	**68.8**
DNAM(v1)	42.3	71.4	81.9	91.8	24.3	41.6	52.4	61.8
PLSAM(v2) [10]	**46.3**	**75.0**	85.6	93.9	26.7	47.9	59.0	68.2
PLSAM(v1) [10]	42.8	71.9	82.0	91.9	23.9	41.8	51.0	61.4
DeepDiff [22]	43.2	68.0	77.6	86.1	-	-	-	-
Null Space [23]	42.3	71.5	82.9	92.1	-	-	-	-
MLAPG [24]	40.7	69.9	82.3	92.4	16.6	33.1	41.2	53.0
DeepList [25]	40.5	69.2	81.0	91.2	-	-	-	-
LOMO+XQDA [17]	40.3	68.3	80.9	91.1	17.3	36.3	44.8	55.4
SCNCD [6]	37.8	68.5	81.2	90.4	-	-	-	-
PKFM [26]	36.8	70.4	83.7	91.7	16.3	35.8	46.0	57.6
CSBT [27]	36.6	66.2	-	88.3	-	-	-	
DCML [28]	33.6	62.9	76.5	87.6	-	-	-	-

Table 1: Results on the VIPeR [1] and QMUL GRID [2, 3, 4] data sets. The best results are shown in bold. (v1) refers to the Weighted LOMO features and XQDA, whereas (v2) refers to the Weighted LOMO features with the Salient Colour Names features and XQDA.

see from Fig 5 that the average Root Mean Squared Error for both the Deep and PLS methods are similar, with only 0.2 pixels between them. Generally, the PLS method varies less from the mean skeleton when compared to the Deep CNN method, which fits limbs in more unusual positions better. The CMC curve is shown in Fig 6.

For CUHK03, we use the manually cropped version of the images. We split the data set into 1160 training identities and 100 testing identities, with only one image of each testing identity present in the testing gallery set.

	CUHK03			
	r=1	r=5	r=10	r=20
DNAM(v2)	62.2	88.0	94.2	97.5
DNAM(v1)	61.9	88.2	94.2	97.5
PLSAM(v2) [10]	**65.2**	**89.8**	**95.0**	97.9
PLSAM(v1) [10]	64.6	89.2	94.9	**98.1**
DeepDiff [22]	62.4	87.9	93.6	96.7
Null Space [23]	58.9	85.6	92.5	96.3
MLAPG [24]	58.0	87.1	94.7	98.0
DeepList [25]	55.9	86.3	93.7	98.0
CSBT [27]	55.5	84.3	-	98.0
LOMO+XQDA [17]	54.9	85.3	92.6	97.1
FPNN [5]	20.7	50.9	67.0	83.0

Table 2: Results on the CUHK03 [5] data set. The best results are shown in bold. (v1) refers to the Weighted LOMO features and XQDA, whereas (v2) refers to the Weighted LOMO features with the Salient Colour Names features and XQDA.

As we do not have any ground-truth, hand-labelled skeleton data for the CUHK03 data set, we instead train the Deep CNN based skeleton fitter on the VIPeR and QMUL GRID data sets. We divide the entire VIPeR and QMUL GRID data sets into training/validation/testing sets as described for the previous two data sets. We train for fifteen epochs with a batch size of 32. However, as the source images for CUHK03 are a higher resolution as compared to VIPeR and QMUL GRID, we instead scale to 160×60 pixels for feature extraction. We run our experiments twenty times, averaging to produce the final results. From Table 2, we can see that the PLS outperforms

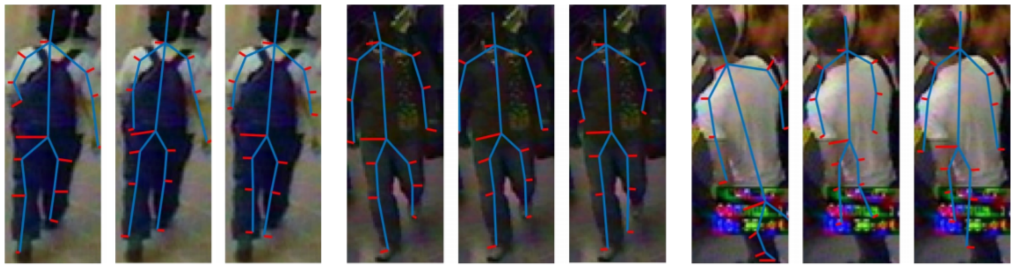

(a) (b) (c)

Figure 5: Examples of ground-truth, deep predicted skeletons and PLS predicted skeletons on the QMUL GRID [2, 3, 4] data set: (a) An example image with a RMSE of 4.3 pixels when using the deep method, and 4.5 pixels when using the PLS method; (b) The image with the minimum RMSE when using the deep method of 2.2 pixels, with the same image having an RMSE of 3.9 pixels when using the PLS method; (c) The image with the maximum RMSE when using the deep method of 18.3 pixels, with the same image having an RMSE of 17.6 pixels when using the PLS method. The average RMSE when using the deep method was 5.5 pixels, with the average when using the PLS method being 5.3 pixels.

the deep method. We believe this is due to it generalising better when an unseen image from an unseen data set is passed to the model. In addition, whilst the VIPeR and QMUL GRID data sets are mainly person images of the front or back of a person, CUHK03 is roughly half frontal or back-facing and half side-facing. The use of a single model for the Deep CNN method versus the two used in the PLS method lead to it fitting a frontal skeleton more often than the PLS method. The CMC curve is plotted in Fig 6.

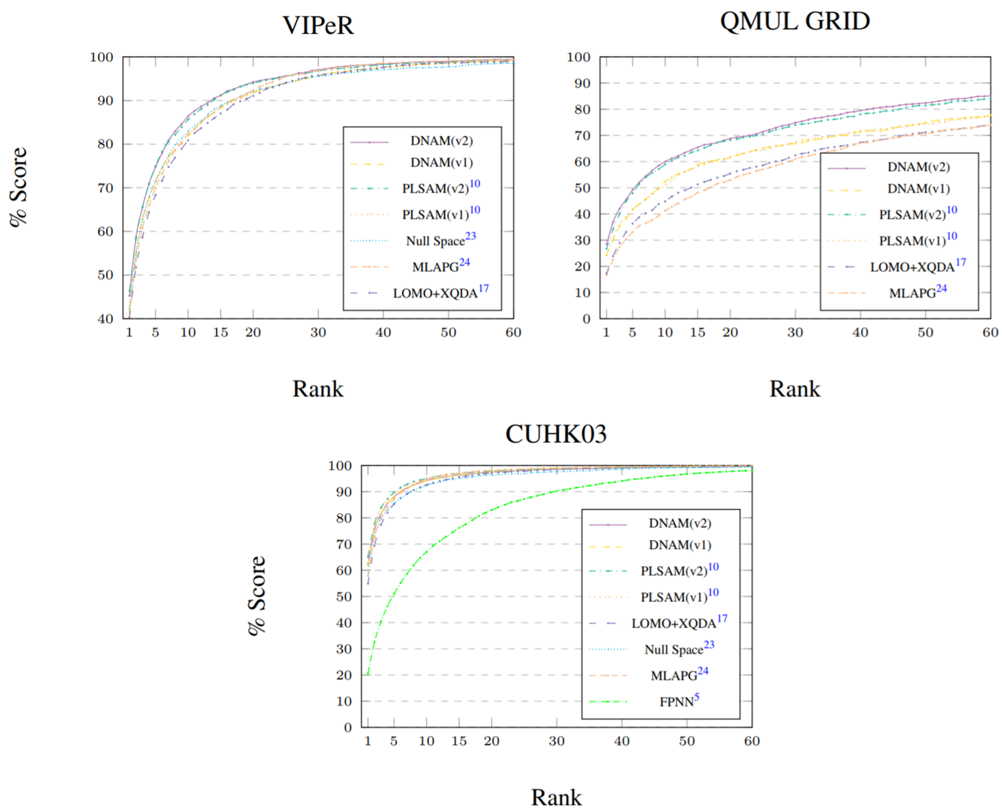

Figure 6: CMC on the VIPeR data set [1], QMUL GRID data set [2, 3, 4] and, CUHK03 data sets [5]. All of our CMC curves are single-shot results. Results are reproduced from [5], [10], [17], [23], [24] and [29].

4 Conclusions

In this paper, we propose a deep CNN based method to fit skeletons to Re-ID images and estimate foreground regions, including head, torso and limbs. We compare the results with a linear appearance based skeleton fitting which uses Partial Least Squares and evaluate the results of both methods in a Re-ID matching framework. For both methods, training images and corresponding ground-truth, hand-labeled skeleton information can be used to build a model to predict the skeleton of a person. From this we have shown that more accurate skeletons can be predicted by using the Deep CNN based model, particularly on unusual person body poses. For the matching, LOMO and Salient Colour Names features are extracted and weighted according to their spatial position in the person image, i.e. ordered by pose information from the foreground estimation. Once extracted, these features are further weighted by XQDA Distance Metric Learning technique for matching. We have demonstrated that by using foreground modelling and weighting the features, we can achieve superior matching performance. Experiments on the VIPeR, QMUL GRID and CUHK03 data sets, and at best our proposed methods achieve 6%, 11.1% and 10.3% improvement respectively when compared to standard approaches using the original LOMO features.

We have also demonstrated that both of our proposed methods generalise well between data sets. Specifically, in the case of CUHK03, we are able to achieve good skeleton fitting results even though the models were trained only on VIPeR and QMUL GRID. This generalisability is important since CNN approaches require large amounts of training data to be accurate. Furthermore, while the PLS method required separate models for frontal and sideways views, the Deep CNN method because of its non-linearities, is able to learn a single model for this task. However, the majority of images used for training the skeleton prediction model were of people facing directly towards or away from the camera, with the occasional sideways-facing image. Future work will investigate how to re-train the model using a more balanced variety of camera directions and skeleton poses, and whether some form of body pose augmentation can be incorporated into the training regime.

An obvious and necessary extension of this work is to combine the deep CNN skeleton prediction into a Deep CNN matching framework, thus precluding the need for feature extraction and distance metric learning. One approach which seems viable is to use the limb localisations to partition the image input into regions of interest boxes extracted and arranged in a grid, which has the advantage that existing deep object matching networks can be usefully leveraged for deep feature learning.

5 Acknowledgements

The authors gratefully acknowledge funding by the UK Engineering and Physical Sciences Research Council (grant no. EP/L016400/1), the EPSRC Centre for Doctoral Training in Urban Science.

References

[1] D. Gray, S. Brennan, and H. Tao, "Evaluating appearance models for recognition, reacquisition, and tracking," in *Proc. IEEE International Workshop on Performance Evaluation for Tracking and Surveillance (PETS)*, **3**(5), 1–7, Citeseer (2007).

[2] C. Liu, S. Gong, C. C. Loy, *et al.*, "Person re-identification: What features are important?," in *European Conference on Computer Vision*, 391–401, Springer (2012).

[3] C. C. Loy, T. Xiang, and S. Gong, "Multi-camera activity correlation analysis," in *Computer Vision and Pattern Recognition, 2009. CVPR*

2009. IEEE Conference on, 1988–1995, IEEE (2009).

[4] C. C. Loy, T. Xiang, and S. Gong, "Time-delayed correlation analysis for multi-camera activity understanding," *International Journal of Computer Vision* **90**(1), 106–129 (2010).

[5] W. Li, R. Zhao, T. Xiao, *et al.*, "Deepreid: Deep filter pairing neural network for person re-identification," in *Proceedings of the IEEE Conference on Computer Vision and Pattern Recognition*, 152–159 (2014).

[6] Y. Yang, J. Yang, J. Yan, *et al.*, "Salient color names for person re-identification," in *European conference on computer vision*, 536–551, Springer (2014).

[7] C. Liu, S. Gong, and C. C. Loy, "On-the-fly feature importance mining for person re-identification," *Pattern Recognition* **47**(4), 1602–1615 (2014).

[8] M. Farenzena, L. Bazzani, A. Perina, *et al.*, "Person re-identification by symmetry-driven accumulation of local features," in *Computer Vision and Pattern Recognition (CVPR), 2010 IEEE Conference on*, 2360–2367, IEEE (2010).

[9] N. Jojic, A. Perina, M. Cristani, *et al.*, "Stel component analysis: Modeling spatial correlations in image class structure," in *Computer Vision and Pattern Recognition, 2009. CVPR 2009. IEEE Conference on*, 2044–2051, IEEE (2009).

[10] G. Watson and A. Bhalerao, "Person re-identification using partial least squares appearance modelling," in *International Conference on Image Analysis and Processing*, 25–36, Springer (2017).

[11] D. Cheng, Y. Gong, S. Zhou, *et al.*, "Person re-identification by multichannel parts-based cnn with improved triplet loss function," in *Proceedings of the IEEE Conference on Computer Vision and Pattern Recognition*, 1335–1344 (2016).

[12] H. Zhao, M. Tian, S. Sun, *et al.*, "Spindle net: Person re-identification with human body region guided feature decomposition and fusion," in *Proceedings of the IEEE Conference on Computer Vision and Pattern Recognition*, 1077–1085 (2017).

[13] L. Wei, S. Zhang, H. Yao, *et al.*, "Glad: Global-local-alignment descriptor for pedestrian retrieval," *arXiv preprint arXiv:1709.04329* (2017).

[14] E. Insafutdinov, L. Pishchulin, B. Andres, *et al.*, "Deepercut: A deeper, stronger, and faster multi-person pose estimation model," in *European Conference on Computer Vision*, 34–50, Springer (2016).

[15] X. Liu, P. Lyu, X. Bai, *et al.*, "Fusing image and segmentation cues for skeleton extraction in the wild," in *Proceedings, ICCV Workshop on Detecting Symmetry in the Wild, Venice*, **6**, 8 (2017).

[16] L.-C. Chen, G. Papandreou, I. Kokkinos, *et al.*, "Deeplab: Semantic image segmentation with deep convolutional nets, atrous convolution, and fully connected crfs," *arXiv preprint arXiv:1606.00915* (2016).

[17] S. Liao, Y. Hu, X. Zhu, *et al.*, "Person re-identification by local maximal occurrence representation and metric learning," in *Proceedings of the IEEE Conference on Computer Vision and Pattern Recognition*, 2197–2206 (2015).

[18] S. Liao, G. Zhao, V. Kellokumpu, *et al.*, "Modeling pixel process with scale invariant local patterns for background subtraction in complex scenes," in *Computer Vision and Pattern Recognition (CVPR), 2010 IEEE Conference on*, 1301–1306, IEEE (2010).

[19] K. He, X. Zhang, S. Ren, *et al.*, "Deep residual learning for image recognition," in *Proceedings of the IEEE conference on computer vision and pattern recognition*, 770–778 (2016).

[20] T. Tieleman and G. Hinton, "Lecture 6.5-rmsprop: Divide the gradient by a running average of its recent magnitude," *COURSERA: Neural networks for machine learning* **4**(2), 26–31 (2012).

[21] M. Koestinger, M. Hirzer, P. Wohlhart, *et al.*, "Large scale metric learning from equivalence constraints," in *Computer Vision and Pattern Recognition (CVPR), 2012 IEEE Conference on*, 2288–2295, IEEE (2012).

[22] Y. Huang, H. Sheng, Y. Zheng, *et al.*, "Deepdiff: Learning deep difference features on human body parts for person re-identification," *Neurocomputing* **241**, 191–203 (2017).

[23] L. Zhang, T. Xiang, and S. Gong, "Learning a discriminative null space for person re-identification," in *Proceedings of the IEEE Conference on Computer Vision and Pattern Recognition*, 1239–1248 (2016).

[24] S. Liao and S. Z. Li, "Efficient psd constrained asymmetric metric learning for person re-identification," in *Proceedings of the IEEE International Conference on Computer Vision*, 3685–3693 (2015).

[25] J. Wang, Z. Wang, C. Gao, *et al.*, "Deeplist: Learning deep features with adaptive listwise constraint for person reidentification," *IEEE Transactions on Circuits and Systems for Video Technology* **27**(3), 513–524 (2017).

[26] D. Chen, Z. Yuan, G. Hua, *et al.*, "Similarity learning on an explicit polynomial kernel feature map for person re-identification," in *Proceedings of the IEEE Conference on Computer Vision and Pattern Recognition*, 1565–1573 (2015).

[27] J. Chen, Y. Wang, J. Qin, *et al.*, "Fast person re-identification via cross-camera semantic binary transformation," in *IEEE Conference on Computer Vision and Pattern Recognition*, (2017).

[28] N. McLaughlin, J. M. del Rincon, and P. C. Miller, "Person reidentification using deep convnets with multitask learning," *IEEE Transactions on Circuits and Systems for Video Technology* **27**(3), 525–539 (2017).

[29] R. Zhao, W. Ouyang, and X. Wang, "Learning mid-level filters for person re-identification," in *Proceedings of the IEEE Conference on Computer Vision and Pattern Recognition*, 144–151 (2014).

Gregory Watson is a PhD candidate at the Department of Computer Science at the University of Warwick, and a member of the Centre for Doctoral Training in Urban Science & Progress. He received his MEng in Computer Science from the University of Warwick in 2015. His current research include using deep learning and foreground modelling to improve person re-identification.

Abhir Bhalerao, PhD, is an Associate Professor in Computer Science at the University of Warwick, UK. He has been an active researcher in medical image analysis and computer vision for over 25 years. He has published around 80 refereed articles in image analysis, medical imaging, graphics and computer vision. His current research interests are in modelling knee and spinal disorders from MRI, biometrics and person re-identification, and vision systems for intelligent vehicles.